Laser driven proton acceleration using resonant nanoantennas

István Papp, Larissa Bravina, Mária Csete, Igor N. Mishustin, Anton Motornenko, Leonid M. Satarov, Horst Stöcker, András Szenes, Dávid Vass, Tamás S. Biró, László P. Csernai, Norbert Kroó
(part of NAPLIFE Collaboration)

ICNFP 2023, July 18, 2023, Kolymbari, Crete

Nanoplasmonic Laser Fusion Research Laboratory

Kőszeg, September 14, 2019 - Int. Workshop on Collectivity
First meeting on the NAPLIFE project (12 people)

Nanoplasmonic Laser Fusion Research Laboratory

Host Institute: Wigner FK
Director General: Lévai Péter
Finance: Vámos-Szigeti Klára

Project scientific leader:
Bíró Tamás Sándor (Wigner)

Project manager:
Szeledi Anett (Wigner)

Book-keeping:
Dömötör Antónia (Wigner)

KIM
NKFIH
FB SZT PIT

Project Governing Body:
Szabó Gábor (ELI-ALPS), chair
Varga Dezső (WFK), secretary
Czitrovszky Aladár (WFK),
Nagy Attila (WFK),
Pohánka Zsuzsa (NKFIH)

Science advisors:
Kroó Norbert, prof. em. (Wigner)
Csernai László, prof. em. (Uni.Bergen)
Johann Rafelski, prof (U. Arizona)

Theory Group:
Csete Mária (SZTE)
Papp István (Wigner FK)
Tóth Emese (SZTE)
Vass Dávid (SZTE)
Szenes András (SZTE)
Bánhelyi Balázs (SZTE)
Czirják András (SZTE)
Földi Péter (SZTE)
Konstantin Zhukovsky (W)

Nanotechnology Group:
Bonyár Attila (BME ETT)
Borók Alexandra (BME ETT)
Szalóki Melinda (DE FOK)
Petrik Péter (EK)
Schereen Zangana (BME)
Janovák László (SZTE)
Tarpataki Nóra (BME)
Kovács Rebeka (BME)

Laser Group:
Kedves Miklós (Wigner)
Aladi Márk (Wigner)
Kumari Archana (Wigner)
Kroó Norbert (Wigner)
Nour Jalal Abdulameer (WFK/DE)
Ráczkevi Béla (Wigner)
Inger Ádádm (Wigner)
Jean-Pierre Svantner (WFK/L)

Spectroscopy Group:
Veres Miklós (Wigner FK)
Rigó István (Wigner FK)
Nagyné Szokol Ágnes (Wigner FK)
Holomb Román (Wigner FK)
Kámán Judit (Wigner FK)
Galbács Gábor (SZTE)
Palásti Ádám (SZTE)
Bélteki Dávid (SZTE)

Thermo-nuclear Fusion

- ηE_f is the usable energy
- The loss is $(1-\eta)(E_0+E_b)$
- $E_0 = 3nkT$, $E_b = bn^2\tau\sqrt{T}$ (thermal bremsstralung)
- Giving the gain factor: $Q = \frac{\eta\epsilon n\tau v\sigma}{4(1-\eta)(3kT+bn\tau\sqrt{T})}$
- Q must be $Q > 1$ for energy production
- This also means $n\tau > \frac{3kT(1-\eta)}{\frac{1}{4}\epsilon\eta\langle v\sigma\rangle - b(1-\eta)\sqrt{T}}$ $\rightarrow$ LC

Lawson criterion

Fulfilling the Lawson criterion

- Magnetically confined plasmas: increase confinement time
- Inertial confinement fusion: increase density of fusion plasma

News on fusion

Home / News / Lawrence Livermore National Laboratory achieves fusion ignition

Dec. 14, 2022

Lawrence Livermore National Laboratory achieves fusion ignition

The U.S. Department of Energy (DOE) and DOE's National Nuclear Security Administration (NNSA) today (Dec. 13) announced the achievement of fusion ignition

News on fusion

Article
https://doi.org/10.1038/s41467-023-36655-1

First measurements of $p^{11}B$ fusion in a magnetically confined plasma

Received: 4 November 2022
Accepted: 10 February 2023
Published online: 21 February 2023
Check for updates

R. M. Magee[1] ✉, K. Ogawa[2], T. Tajima[1,3], I. Allfrey[1], H. Gota[1], P. McCarroll[1], S. Ohdachi[2], M. Isobe[2], S. Kamio[1,3], V. Klumper[1,3], H. Nuga[2], M. Shoji[2], S. Ziaei[1], M. W. Binderbauer[1] & M. Osakabe[2]

Proton-boron ($p^{11}B$) fusion is an attractive potential energy source but technically challenging to implement. Developing techniques to realize its potential requires first developing the experimental capability to produce $p^{11}B$ fusion in the magnetically-confined, thermonuclear plasma environment. Here we report clear experimental measurements supported by simulation of $p^{11}B$ fusion with high-energy neutral beams and boron powder injection in a high-temperature fusion plasma (the Large Helical Device) that have resulted in diagnostically significant levels of alpha particle emission. The injection of boron powder into the plasma edge results in boron accumulation in the core. Three 2 MW, 160 kV hydrogen neutral beam injectors create a large population of well-confined, high -energy protons to react with the boron plasma. The fusion products, MeV alpha particles, are measured with a custom designed particle detector which gives a fusion rate in very good relative agreement with calculations of the global rate. This is the first such realization of $p^{11}B$ fusion in a magnetically confined plasma.

The proton–boron fusion reaction ($p^{11}B$),

While the challenges of producing the fusion core are greater for

News on fusion

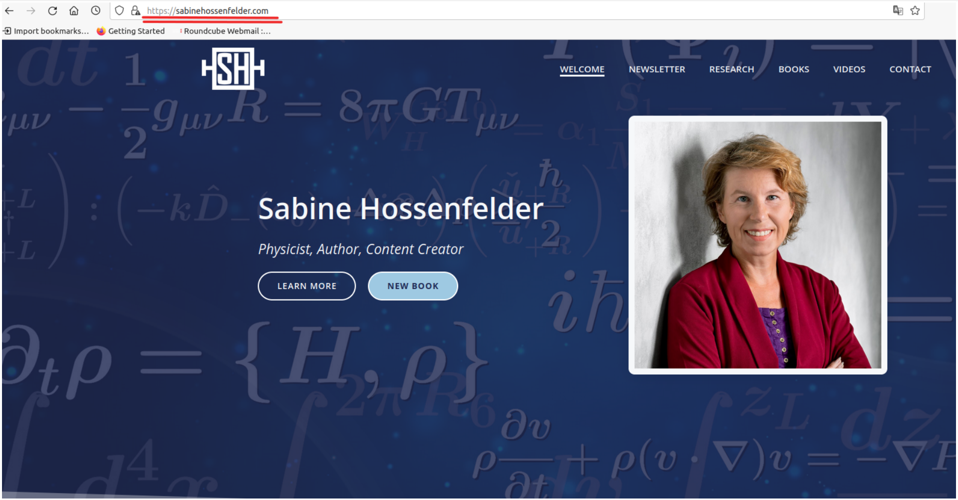

Direct vs Indirect drive

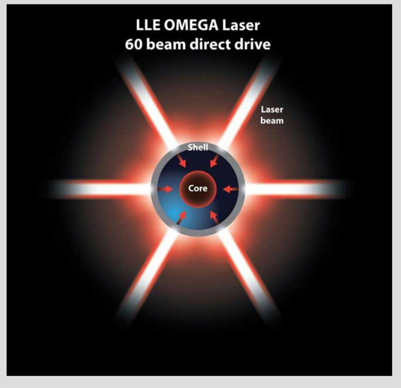

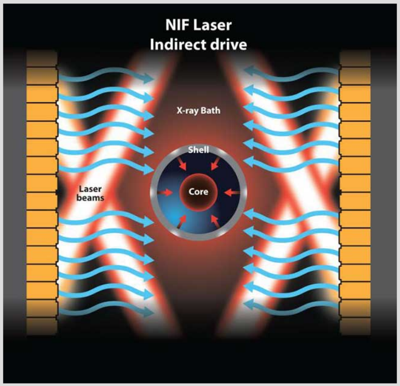

PHOTONICS MEDIA photonics.com

Hohlraum

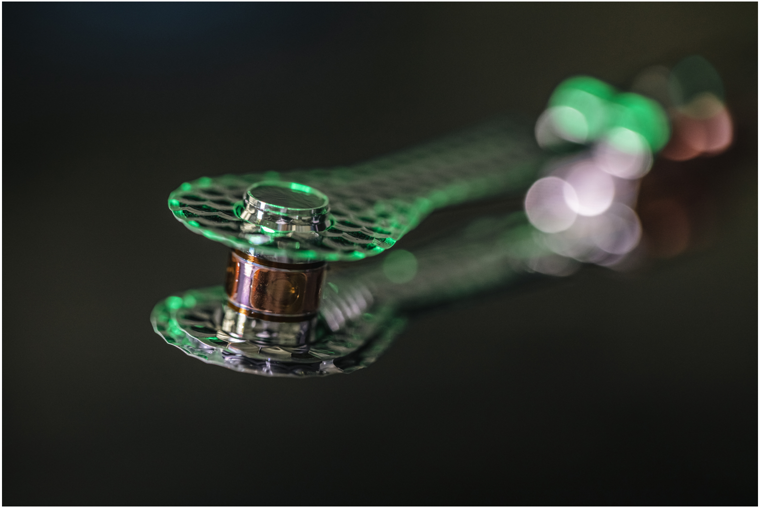

Hohlraum 2014

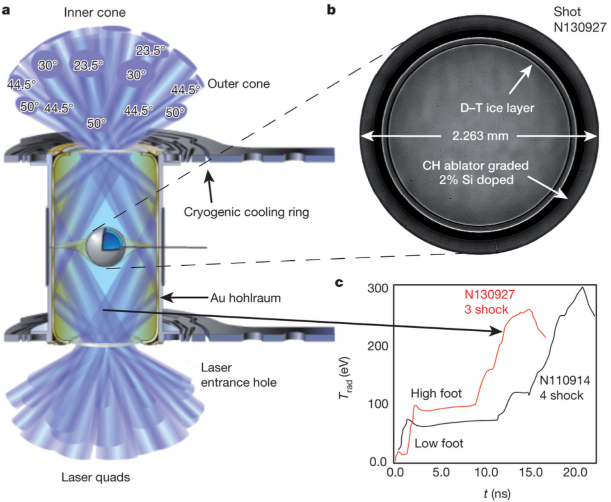

[O.A. Hurricane et al., Nature, 506, 343 (2014)]

Hohlraum 2022

Fig. 1: Schematic of the indirect-drive inertial confinement approach to fusion.

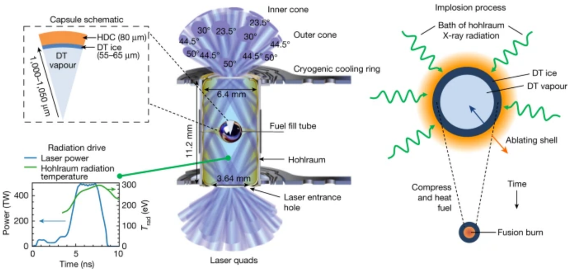

Centre, A typical indirect-drive target configuration with key engineering elements labelled. Laser beams (blue) enter the hohlraum through laser entrance holes at various angles. Top left, A schematic pie diagram showing the radial distribution and dimensions of materials in diamond (high-density carbon, HDC) ablator implosions. Bottom left, The temporal laser power pulse-shape (blue) and associated hohlraum radiation temperature (green). Right, At the centre of the hohlraum, the capsule

[A.B, Zylstra, O.A. Hurricane et al., Nature, 601, 542-548 (2022)]

Rayleigh-Taylor instabilities

Rayleigh-Taylor instabilities

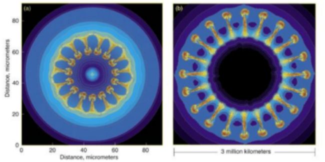

Striking similarities exist between hydrodynamic instabilities in (a) inertial confinement fusion capsule implosions and (b) core-collapse supernova explosions. [Image (a) is from Sakagami and Nishihara, *Physics of Fluids B* **2**, 2715 (1990); image (b) is from Hachisu et al., *Astrophysical Journal* **368**, L27 (1991).]

Energy must be delivered as sysmmetric as possible!

Different levels of corrugation of the shell surfaces :

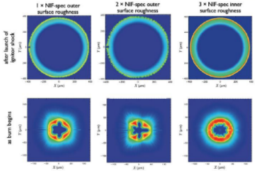

Left: same roughness of inner and outer surface as specified for the NIF target
Center: outer surface roughness is twice the NIF level
Right: DT inner surface roughness three times larger than NIF specifications

[S. Atzeni et al., Nucl. Fusion 54, 054008 (2014).] 25

Latest (January 2023) news 3.15MJ kinetic energy at NIF with burning time of 89-137 ps(?)

RFD

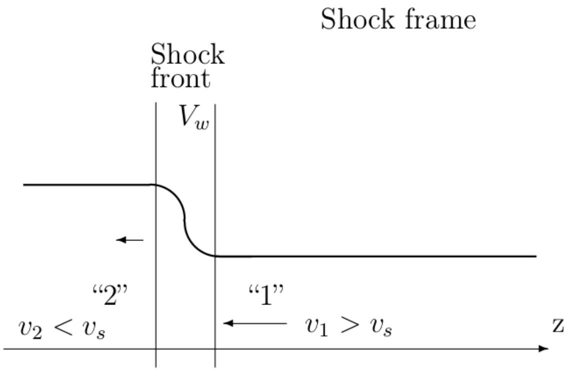

[Csernai, L.P. (1987). Detonation on a time-like front for relativistic systems. Zh. Eksp. Teor. Fiz. 92, 379-386.]

RFD

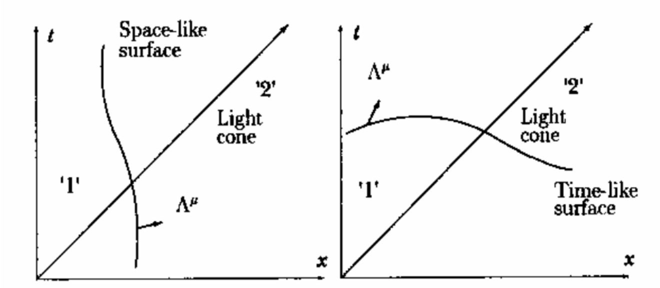

Figure 5.9: Space-like (a) and time-like (b) surfaces of discontinuity

[Csernai, L.P. (1987). Detonation on a time-like front for relativistic systems. Zh. Eksp. Teor. Fiz. 92, 379-386.]

RFD

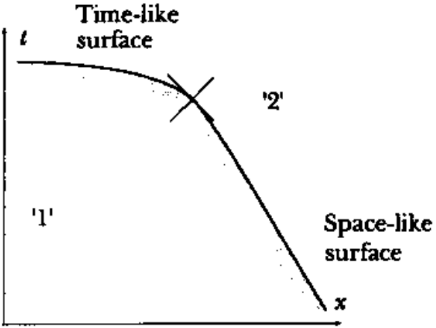

Figure 5.10: Smooth change from spacelike to timelike detonation

[Csernai, L.P. (1987). Detonation on a time-like front for relativistic systems. Zh. Eksp. Teor. Fiz. 92, 379-386.]

Constant absorptivity

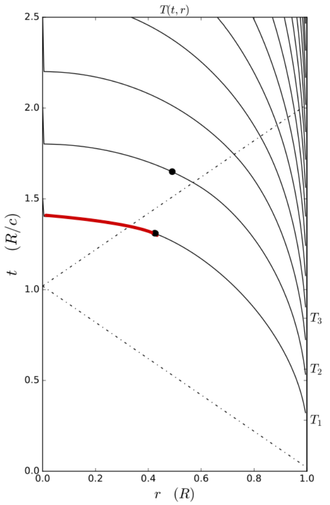

[L.P. Csernai & D.D. Strottman, Laser and Particle Beams 33, 279 (2015)]

$\alpha_{k_{middle}} = \alpha_{k_{edge}}$

Simultaneous volume ignition is only up to 12%

Changing absorptivity

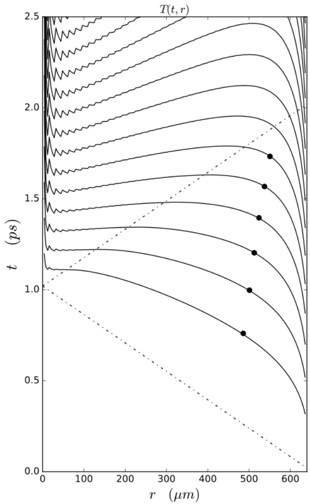

[Csernai, L.P., Kroo, N. and Papp, I. (2017). Procedure to improve the stability and efficiency of laser-fusion by nano-plasmonics method. Patent P1700278/3 of the Hungarian Intellectual Property Office.]

$\alpha_{k_{middle}} \approx 4 \times \alpha_{k_{edge}}$

Simultaneous volume ignition is up to 73%

Flat target

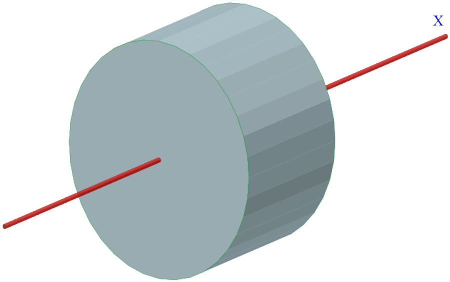

Schematic view of the cylindrical, flat target of radius, R, and thickness, h.
$V = 2\pi R^3$, $R = \sqrt[3]{V/(2\pi)}$, $h = \sqrt[3]{4V/\pi}$.

[L.P. Csernai, M. Csete, I.N. Mishustin, A. Motornenko, I. Papp, L.M. Satarov, H. Stöcker & N. Kroó, Radiation- Dominated Implosion with Flat Target, *Physics and Wave Phenomena*, **28** (3) 187-199 (2020)]

Varying absorptivity

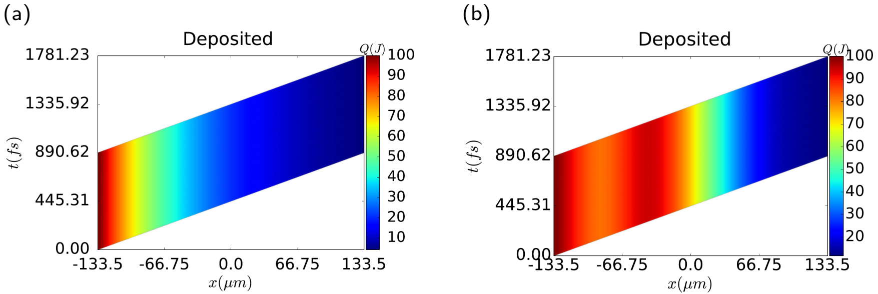

Deposited energy per unit time in the space-time plane across the depth, *h*, of the flat target. **(a) without** nano-shells **(b) with** nano-shells

To increase central absorption we used the following distribution:

$$\alpha_{ns}(s) = \alpha_{ns}^{C} + \alpha_{ns}(0) \cdot \exp\left[4 \times \frac{\left(\frac{s}{100}\right)^2}{\left(\frac{s}{100} - 1\right)\left(\frac{s}{100} + 1\right)}\right] .$$

Similar Configuration with success

Nuclear probes of an out-of-equilibrium plasma at the highest compression **Phys. Lett. A 383 (2019) 2285-2289.**

G. Zhang[a,b,*], M. Huang[c], A. Bonasera[d,e,*], Y.G. Ma[f,b,i,*], B.F. Shen[g,h,*], H.W. Wang[a,b], W.P. Wang[g], J.C. Xu[g], G.T. Fan[a,b], H.J. Fu[b], H. Xue[b], H. Zheng[j], L.X. Liu[a,b], S. Zhang[c], W.J. Li[b], X.G. Cao[a,b], X.G. Deng[b], X.Y. Li[b], Y.C. Liu[b], Y. Yu[g], Y. Zhang[b], C.B. Fu[k], X.P. Zhang[k]

4 (up) + 4(down) lasers
Target thickness, h (3.6μm-1mm) & radius, R, (150-400μm) were varied.

Total pulse energy 1.2kJ (2ns) for 8 beams.
Shortest (250ps) pulses -> 100s MeV ions > non-thermal distr. = directed ion acceleration

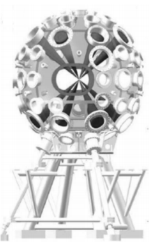

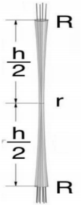

Typical fusion neutron energies were measured & used to extract the target density.

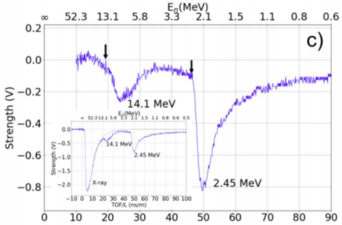

33

Nanoplasmonic Laser Fusion Research Laboratory

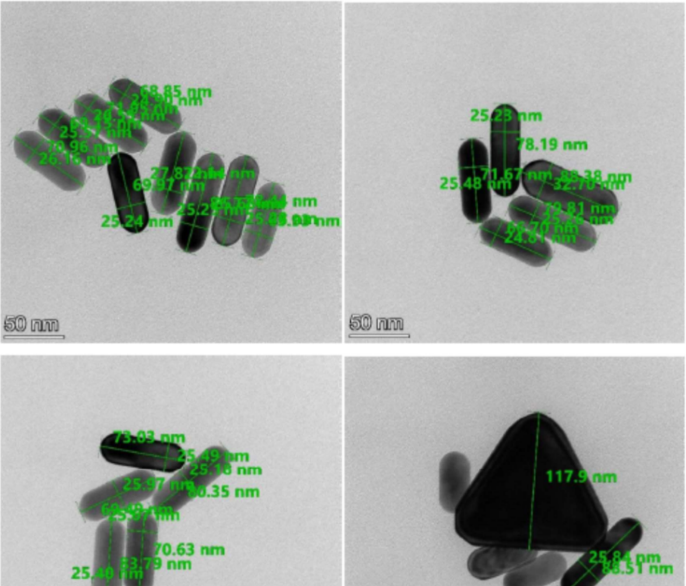

Transmission Electron-microscopy photos of 75x25 nm gold nano-rod antennas

[Judit Kámán, A. Bonyár et al. (NAPLIFE Collab.)., Gold nanorods ..., 10th ICNFP 2021, **Kolymbari]**

Nanorod

Field solver:
$\epsilon(\omega) = 1 - \frac{\omega_p^2}{(\omega^2 + i\gamma\omega)}$
where ω_p is the plasma frequency: $\sqrt{\frac{n_e e^2}{m' \epsilon_0}}$
γ is the damping factor or collision frequency: $\gamma = \frac{1}{\tau}$ and τ is the average time between collisions
Particle simulation:

$$\frac{\partial \boldsymbol{E}}{\partial t} = \frac{1}{\mu_0 \epsilon_0} \nabla \times \boldsymbol{B} - \frac{\boldsymbol{J}}{\epsilon_0}, \ \frac{\partial \boldsymbol{B}}{\partial t} = -\nabla \times \boldsymbol{E}$$

$\gamma_i m_i \boldsymbol{v}_i = q_i(\boldsymbol{E}_i + \boldsymbol{v}_i \times \boldsymbol{B}_i)$, γ_i is the relativistic factor

Nanorod

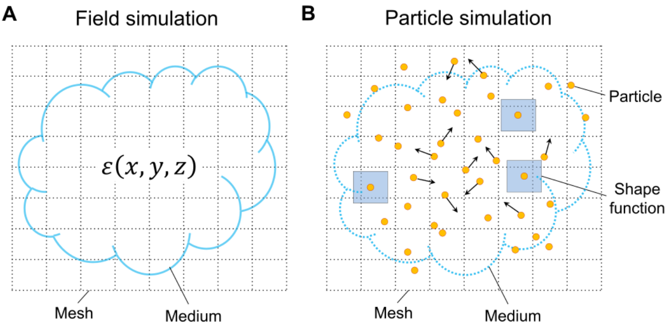

[W. J. Ding,et al., Particle simulation of plasmons Nanophotonics, vol. 9, no. 10, pp. 3303-3313 (2020)]

Particle In Cell methods

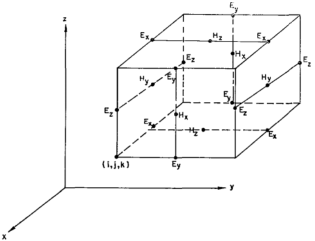

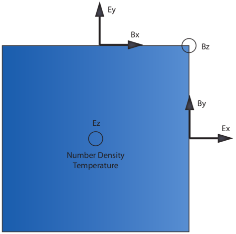

Figure 2: The Yee grid in 2D

[F.H. Harlow (1955). A Machine Calculation Method for Hydrodynamic Problems. Los Alamos Scientific Laboratory report LAMS-1956]

[T.D. Arber et al 2015 Plasma Phys. Control. Fusion 57 113001]

A **super-particle** (**marker-particle**) is a computational particle that represents many real particles.

Particle **mover** or **pusher** algorithm as (typically Boris algorithm).

Finite-difference time-domain method for solving the time evolution of **Maxwell's equations**.

General layout of the EPOCH code

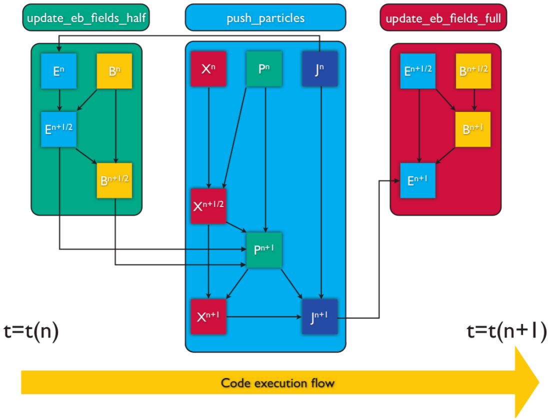

[EPOCH 4.0 dev manual]

- (input) deck
- housekeeping
- io
- parser
- physics_packages
- user_interaction

FDTD in EPOCH

- $\boldsymbol{E}_{n+\frac{1}{2}} = \boldsymbol{E}_n + \frac{\Delta t}{2}\left(c^2\nabla \times \boldsymbol{B}_n - \frac{\boldsymbol{j}_n}{\epsilon_0}\right)$
- $\boldsymbol{B}_{n+\frac{1}{2}} = \boldsymbol{B}_n - \frac{\Delta t}{2}\left(\nabla \times \boldsymbol{E}_{n+\frac{1}{2}}\right)$
- Call particle pusher which calculates j_{n+1}
- $\boldsymbol{B}_{n+1} = \boldsymbol{B}_{n+\frac{1}{2}} - \frac{\Delta t}{2}\left(\nabla \times \boldsymbol{E}_{n+\frac{1}{2}}\right)$
- $\boldsymbol{E}_{n+1} = \boldsymbol{E}_{n+\frac{1}{2}} + \frac{\Delta t}{2}\left(c^2\nabla \times \boldsymbol{B}_{n+1} - \frac{\boldsymbol{j}_{n+1}}{\epsilon_0}\right)$

Particle pusher

- Solves the relativistic equation of motion under the Lorentz force for each marker-particle

$$\boldsymbol{p}_{n+1} = \boldsymbol{p}_n + q\Delta t \left[\boldsymbol{E}_{n+\frac{1}{2}} \left(\boldsymbol{x}_{n+\frac{1}{2}} \right) + \boldsymbol{v}_{n+\frac{1}{2}} \times \boldsymbol{B}_{n+\frac{1}{2}} \left(\boldsymbol{x}_{n+\frac{1}{2}} \right) \right]$$

  $\boldsymbol{p}$ is the particle momentum q is the particle's charge $\boldsymbol{v}$ is the velocity.
  $\boldsymbol{p} = \gamma m \boldsymbol{v}$, where m is the rest mass $\gamma = \left[(\boldsymbol{p}/mc)^2 + 1 \right]^{1/2}$

- Villasenor and Buneman current deposition scheme [Villasenor J & Buneman O 1992 Comput. Phys. Commun. 69 306], always satisfied: $\nabla \cdot \boldsymbol{E} = \rho/\epsilon_0$, where ρ is the charge density.

Particle shape

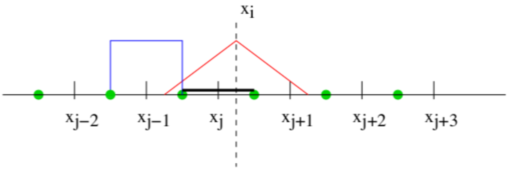

Figure 3: Second order particle shape function

First order approximations are considered

$$F_{part} = \frac{1}{2}F_{i-1}\left(\frac{1}{2}+\frac{x_i - X}{\Delta x}\right)^2 + \frac{1}{2}F_i\left(\frac{3}{4}-\frac{(x_i - X)^2}{\Delta x^2}\right)^2 + \frac{1}{2}F_{i+1}\left(\frac{1}{2}+\frac{x_i - X}{\Delta x}\right)^2$$

[EPOCH 4.0 dev manual]

Metal Nanoparticles as Plasmas in Vacuum

The conduction band electrons in metals behave as strongly coupled plasmas.
For golden nanorods of 25nm diameter in vacuum this gives an effective wavelength of $\lambda_{eff} = 266\text{nm}$

$$\frac{\lambda_{eff}}{2R\pi} = 13.74 - 0.12[\varepsilon_\infty + 141.04] - \frac{2}{\pi} + \frac{\lambda}{\lambda_p} 0.12\sqrt{\varepsilon_\infty + 141.04}$$

[Lukas Novotny, Effective Wavelength Scaling for Optical Antennas, Phys. Rev. Lett. **98**, 266802 (2007).]

Metal Nanoparticles as Plasmas in UDMA-Tegdma

For golden nanorods of 25nm diameter in vacuum this gives an effective wavelength of $\lambda_{eff}/2 = 85$nm
The **propagation** velocity of light **inside** the **medium** is reduced to $c_s = c/\sqrt{\varepsilon_s}$, where $\varepsilon_s = n^2$.

$$\frac{\lambda_{eff}}{2R\pi} = 13.74 - 0.12[\varepsilon_\infty + \varepsilon_s 141.04]/\varepsilon_s - \frac{2}{\pi} + \frac{\lambda}{\lambda_p} 0.12\sqrt{\varepsilon_\infty + \varepsilon_s 141.04}/\varepsilon_s$$

[Lukas Novotny, Effective Wavelength Scaling for Optical Antennas, Phys. Rev. Lett. **98**, 266802 (2007).]

Kinetic Modelling of the Nanorod

Nanorod inside a PIC simulation box

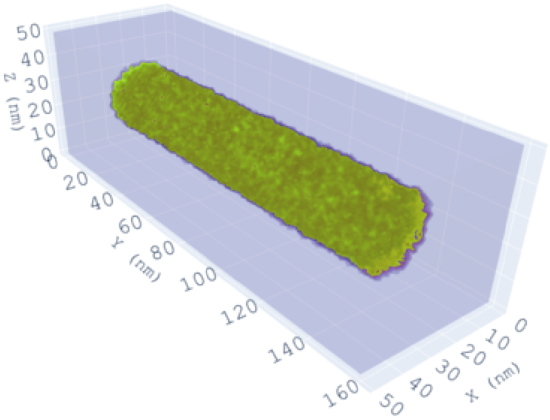

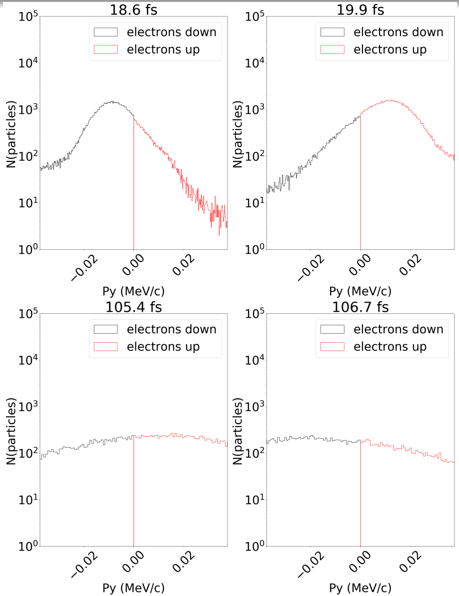

Considerations for the simulation box:
$S_{CB} = 530 \times 530\text{nm}^2 = 2.81 \times 10^{-9}\text{cm}^2$ and length of $L_{CB} = 795\text{nm}$

beam crosses the box in $T = 795\text{nm}/c = 2.65\text{fs}$

Nanorod size: 25 nm diameter with 130 nm length

Pulse length: $40\times\lambda/c = 106$ fs
Intensity: 4×10^{15} W/cm^2
[Papp I, Bravina L, Csete M, Kumari A, et al. Kinetic model evaluation of the resilience of plasmonic nanoantennas for laser-induced fusion. PRX Energy (2022)]

Kinetic Modelling of the Nanorod

Evolution of the nanoantenna

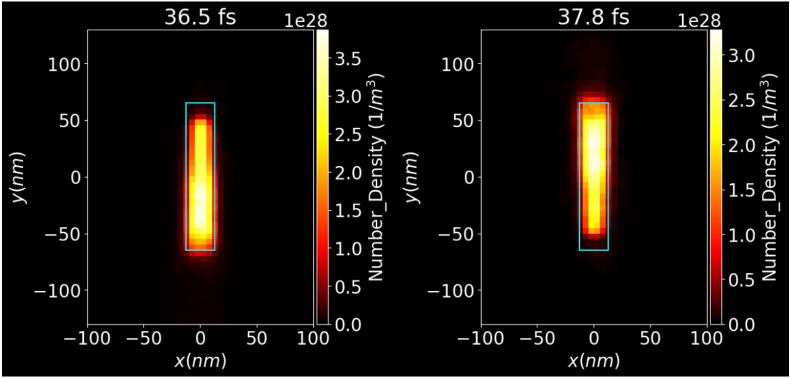

Number density of electrons in the middle of a nanorod of size 25x130 nm at different times. The nanorod is orthogonal to the beam direction, x.

Kinetic Modelling of the Nanorod in Vacuum

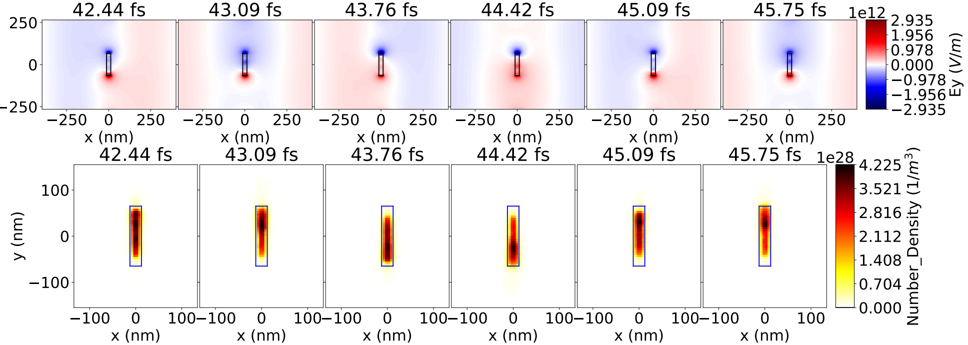

- Evolution of the *E* field's *y* component from 42.4 till 45.7 fs, around a nanorod of 25x130 nm.
- The direction of the *E* field at the two ends of the nanorod does not change.

In Vacuum

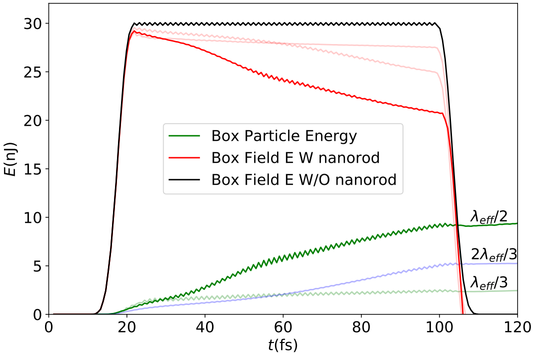

energy in the box **without nanorod** antenna 3×10^{-8} J (black line)
nanorod absorbs EM energy reducing it to 2.3×10^{-8} J (red line)
deposited energy in the nanorod (green line)
results in light absorption cross section highest

In UDMA-TEGDMA copolymer comparison

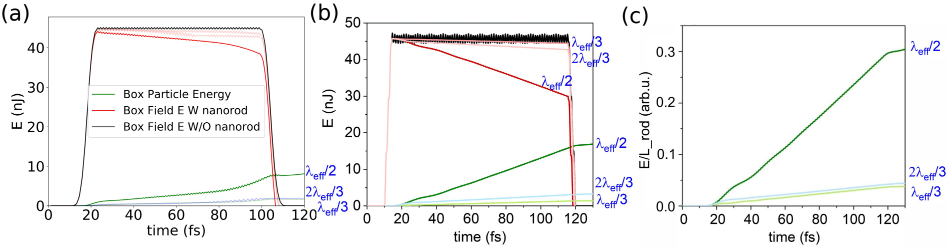

Optical response of the gold nanorod with different numerical methods and lengths, $L = \lambda_{eff}/2, \lambda_{eff}/3 and 2\lambda_{eff} eff/3$. (a) PIC, (b) FEM and (c) FEM with normalized values to unit antenna length.
[I. Papp, L. Bravina, M. Csete, et al.(NAPLIFE Collaboration), Kinetic model of resonant nanoantennas in polymer for laser induced fusion, Frontiers in Physics, **11**, 1116023 (2023).]

In UDMA-TEGDMA copolymer comparison

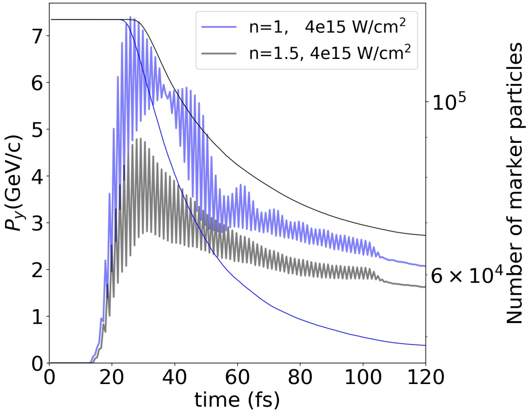

Time dependence of the **total** polarity directed **momentum** of the conducting electrons in the nanorod.

[I. Papp, L. Bravina, M. Csete, et al.(NAPLIFE Collaboration), Kinetic model of resonant nanoantennas in polymer for laser induced fusion, Frontiers in Physics, **11**, 1116023 (2023).]

In UDMA-TEGDMA copolymer comparison

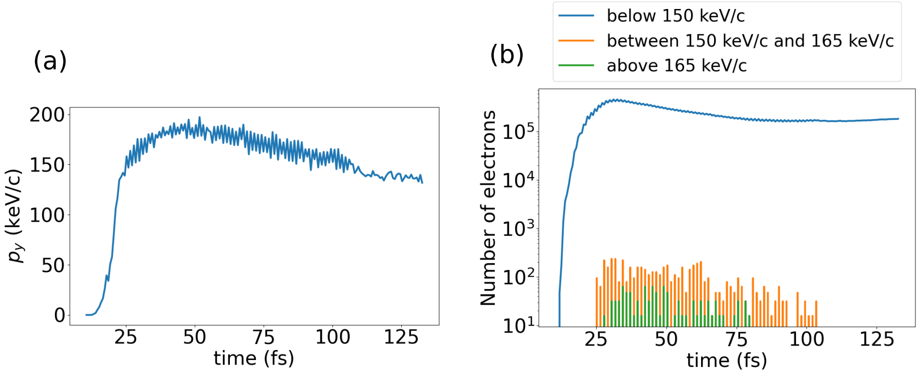

Electrons leaving the nanorod. Figure (a) indicates the **maximum momentum** in time, Figure (b) shows the distribution of electrons at different momentum values.

[I. Papp, L. Bravina, et al. Frontiers in Physics, **11**, 1116023 (2023).]

Capping in the experiment

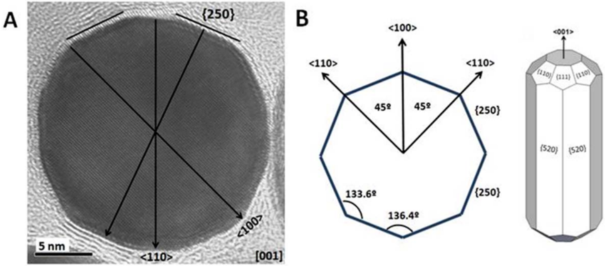

The gold nanorods in the polymer matrix are coated with dodecanethiol (DDT) capping. $CH_3(CH_2)_{11}SH$
[Bonyár A, et al.The Effect of Fem- tosecond Laser Irradiation and Plasmon Field on the Degree of Conversion of a UDMA-TEGDMA Copoly- mer Nanocomposite Doped with Gold Nanorods. Inter- national Journal of Molecular Sciences 23(21), 13575 (2022).]

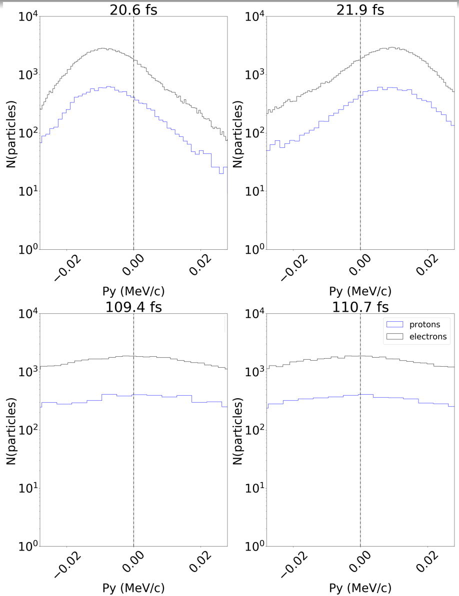

Considerations for the simulation box:
$S_{CB} = 530 \times 530\text{nm}^2 = 2.81 \times 10^{-9}\text{cm}^2$ and length of $L_{CB} = 795\text{nm}$

beam crosses the box in $T = 795\text{nm}/c = 2.65\text{fs}$

Nanorod size: **25 nm diameter with 85 nm length**

Pulse length: $40 \times \lambda/c = 106$ fs
Intensity: 4×10^{15} W/cm^2

Ionisable surrounding

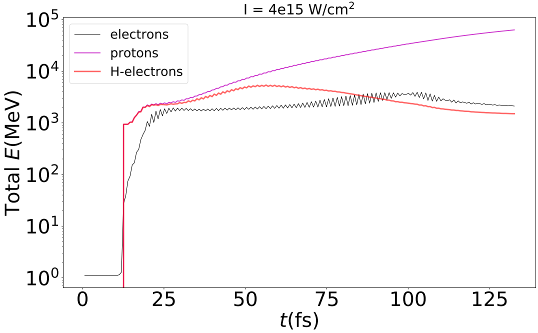

We consider a laser pulse of intensity $I = 4 \cdot 10^{15}\text{W}/\text{cm}^2$ and $I = 4 \cdot 10^{17}\text{W}/\text{cm}^2$ and duration of 106fs.

Ionisable surrounding

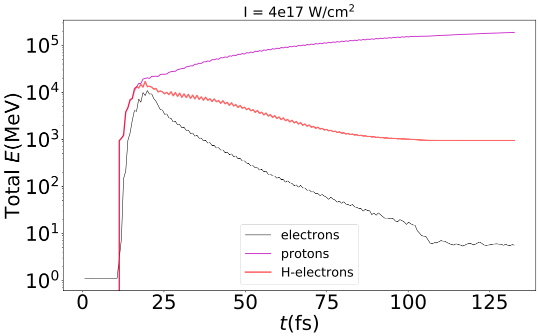

We consider a laser pulse of intensity $I = 4 \cdot 10^{15}\text{W}/\text{cm}^2$ and $I = 4 \cdot 10^{17}\text{W}/\text{cm}^2$ and duration of 106fs.

Ionisable surrounding

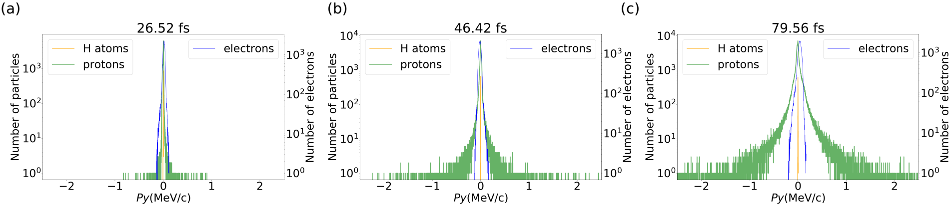

The number of electrons and protons when they leave the nano antennas or their surrounding at intensity $\mathrm{I} = 4 \times 10^{15}\ \mathrm{W/cm^2}$.

Ionisable surrounding

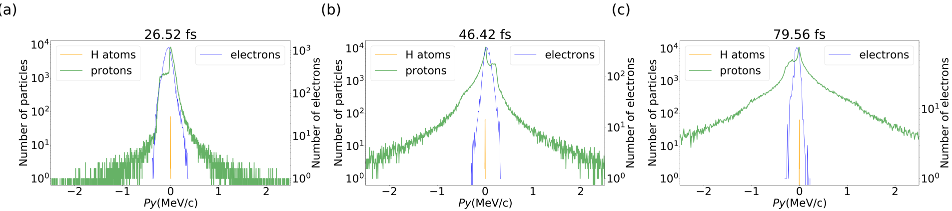

The number of electrons and protons when they leave the nano antennas or their surrounding at intensity $I = 4 \times 10^{17}$ W/cm^2.

Conclusions, Looking forward

- The model is in good agreement with currently available widely accepted methods
- Quantitative differences mainly come at different resonant lengths
- The model is less idealized than before
- Ionization in the medium is now included, nuclear reactions are on the way
- Target pre-compression in the next step can be estimated

Acknoledgements

Enlightening discussions with Johann Rafelski are gratefully acknowledged. Horst Stöcker acknowledges the Judah M. Eisenberg Professor Laureatus chair at Fachbereich Physik of Goethe Universität Frankfurt. We would like to thank the **Wigner GPU Laboratory at the Wigner Research Center for Physics** for providing support in computational resources. This work is supported in part by the Frankfurt Institute for Advanced Studies, Germany, the Eötvös Loránd Research Network of Hungary, the Research Council of Norway, grant no. 255253, and the National Research, Development and Innovation Office of Hungary, via the projects: Nanoplasmonic Laser Inertial Fusion Research Laboratory (NKFIH-468-3/2021), Optimized nanoplasmonics (K116362), and Ultrafast physical processes in atoms, molecules, nanostructures and biological systems (EFOP-3.6.2-16-2017-00005). LP acknowledges support from Wigner RCP, Budapest (2022-2.2.1-NL-2022-00002).

We also greatly acknowledge **you**r attention!